Unified pre- and postsynaptic long-term plasticity enables reliable and flexible learning

Citation for published version:
Costa, RP, Froemke, RC, Sjöström, PJ & Van Rossum, MCW 2015, 'Unified pre- and postsynaptic long-term plasticity enables reliable and flexible learning', *eLIFE*, vol. 4. https://doi.org/10.7554/eLife.09457

Digital Object Identifier (DOI):
10.7554/eLife.09457

Link:
Link to publication record in Edinburgh Research Explorer

Document Version:
Peer reviewed version

Published In:
eLIFE

ACCEPTED MANUSCRIPT

Unified pre- and postsynaptic long-term plasticity enables reliable and flexible learning

Rui Ponte Costa, Robert C Froemke, Per Jesper Sjöström, Mark C W van Rossum

DOI: http://dx.doi.org/10.7554/eLife.09457

Cite as: eLife 2015;10.7554/eLife.09457

Received: 15 June 2015
Accepted: 25 August 2015
Published: 26 August 2015

Unified pre- and postsynaptic long-term plasticity enables reliable and flexible learning

Rui Ponte Costa[1,2], Robert C. Froemke[3,4], P. Jesper Sjï¿œstrï¿œm[5*] and Mark C. W. van Rossum[1*]

26th August 2015

[1]Institute for Adaptive and Neural Computation, School of Informatics
University of Edinburgh, Edinburgh, UK
[2]Centre for Neural Circuits and Behaviour
University of Oxford, Oxford, UK
[3]Skirball Institute for Biomolecular Medicine
Departments of Otolaryngology, Neuroscience and Physiology
New York University School of Medicine, New York, NY, USA
[4]Center for Neural Science
New York University, New York, NY, USA
[5]The Research Institute of the McGill University Health Centre
Department of Neurology and Neurosurgery
McGill University, Montreal, Canada
[*]These authors contributed equally to this work.

Abstract

Although it is well known that long-term synaptic plasticity can be expressed both pre- and postsynaptically, the functional consequences of this arrangement have remained elusive. We show that spike-timing-dependent plasticity with both pre- and postsynaptic expression develops receptive fields with reduced variability and improved discriminability compared to postsynaptic plasticity alone. These long-term modifications in receptive field statistics match recent sensory perception experiments. Moreover, learning with this form of plasticity leaves a hidden postsynaptic memory trace that enables fast re-learning of previously stored information, providing a cellular substrate for memory savings. Our results reveal essential roles for presynaptic plasticity that are missed when only postsynaptic expression of long-term plasticity is considered, and suggest an experience-dependent distribution of pre- and postsynaptic strength changes.

Survival depends on learning accurate actions in response to sensory stimuli while remaining capable to quickly adapt in dynamic environments. The neural substrate of learning is believed to be long-term synaptic plasticity [1, 2]. After decades of debate [3, 4], it has become increasingly clear that expression of long-term synaptic plasticity can be either pre- or postsynaptic or both [5, 6, 7, 8, 9]. However, the functional consequences of this segregation into pre- and postsynaptically expressed plasticity have remained unclear. To investigate this, we developed a biologically tuned spike-timing-dependent plasticity (STDP) model, that in contrast to earlier models [10, 11, 12, 13, 14, 15, 16, 17, 18, 19, 20], involves both loci of expression.

Inspired by earlier work [11, 14], this phenomenological model relies on exponentially decaying traces of the pre- and postsynaptic spike trains, X and Y (Figure 1a,b). The presynaptic trace x_+ tracks past presynaptic activity, e.g. glutamate binding to postsynaptic NMDA receptors. When presynaptic activity x_+ is rapidly followed by postsynaptic spikes, unblocking NMDA receptors, postsynaptically expressed long-term potentiation (LTP) is triggered and increases the postsynaptic factor q, which can be interpreted as the quantal amplitude. Conversely, the postsynaptic trace y_+ represents prior postsynaptic activity, e.g. retrograde nitric oxide signalling, which when paired with presynaptic spikes leads to presynaptically expressed LTP [7]. Finally, the trace y_- tracks postsynaptic activity such as endocannabinoid retrograde release and elicits presynaptically expressed long-term depression (LTD) when coincident with presynaptic spikes [21]. Presynaptically expressed plasticity is conveyed by long-term changes in the presynaptic factor P [22], which can be interpreted as the presynaptic release probability (see Material and methods).

The model parameters were tuned to an extensive data set of plasticity experiments of monosynaptic connections between neocortical layer-5 pyramidal cells [23, 7, 21]. Homeostatic scaling of the postsynaptic amplitude q was included to counterbalance postsynaptic potentiation (see Material and methods) [24]. The resulting model not only captures the timing and frequency dependence of the synaptic strength changes (Figure 1c and Figure 1 - figure supplement 1), but also its pre- as well as postsynaptic expression (Figure 1d, e). It thus captures the observed cross-scale interactions between short and long-term synaptic plasticity [21, 7]. Short-term depression becomes stronger after LTP and weaker after LTD (Figure 1f,g). We validated the model against experiments with pharmacological blockade of presynaptic LTD or LTP (see Material and methods). Abolishing presynaptic LTP by nitric oxide blockade reduced total potentiation as only the postsynaptic potentiation component was left [7]. Likewise, with the presynaptic trace y_+ disabled, presynaptic LTP was blocked, while the synaptic dynamics remained unchanged (Figure 1h and Figure 1 - figure supplement 3a). Conversely, simulated blockade of presynaptic LTD during LTP induction gave rise to stronger presynaptic potentiation and short-term depression, as observed experimentally during endocannabinoid blockade [7] (Figure 1h and Figure 1 - figure supplement 3b).

Figure 1: Unified model of pre- and postsynaptically expressed STDP. (**a**) The synaptic weight is the product of a presynaptic factor P and a postsynaptic factor q. Long-term modifications in P and q are governed by interactions between the pre- and postsynaptic spike trains. (**b**) Model example in which the postsynaptic neuron first spikes three times at 20 Hz (Y) $\Delta t = +10$ms after the presynaptic neuron (X), leading to LTP by increasing both q and P. Next, when the relative timing Δt is reversed, LTD results as P weakens strongly, even though q still slightly strengthens. (**c**) The model fits the rate dependence of synaptic plasticity (squares, [23]) for both positive (blue: +10ms) and negative timings (red: -10ms). (**d**,**e**) The changes in the pre- and postsynaptic factors P and q match experimental data (reanalyzed from [23]; see Material and methods and Figure 1 - figure supplement 2). (**f**,**g**) As in experiments (top), short-term depression in the model is reduced after LTD (20 Hz, $\Delta t = -10$ms) and increased after LTP (50 Hz, $\Delta t = +10$ms) (bottom). Experimental traces from [21] (f) and from [7] (g). (**h**) Model (blue) is consistent with LTP experiments (black) [7] in control conditions, nitric oxide (NO) blockade, and endocannabinoid (eCB) blockade. NO and eCB antagonists abolish and promote presynaptic LTP, respectively [7].

We first investigated the functional consequences of unified pre- and postsynaptically expressed STDP on the postsynaptic responses during cortical receptive field development. We simulated receptive field development of a postsynaptic neuron receiving 100 synaptic inputs (Material and methods). Presynaptic activity was described by Poisson processes with rates spatially distributed according to a Gaussian profile (Figure 2a). We defined inputs near the peak of the Gaussian profile as *on*, and those far away from the peak as *off*. After learning, *on* neurons had increased q and P, while *off* neuron had reduced q and P (Figure 2a). During learning, the changes in q are preceded by changes in P (Figure 2c). To quantify the effect of the plasticity on the postsynaptic neuron, we stimulate a given input and calculated the signal-to-noise ratio (SNR) of the first postsynaptic response amidst background noise (see Material and methods). A high SNR means that the response can be easily distinguished from the background. After learning, only *on* inputs had developed a high SNR (Figure 2b). Although both high and low P yielded low variance (Figure 2 - figure supplement 1), high P was required for high SNR (Figure 2c).

To further assess the discriminability of the first postsynaptic response, we used classification analysis (see Material and methods), which revealed that *on* inputs obtained a near-perfect discrimination (Figure 2d) over a range of background noise levels (Figure S4). However, a model with only postsynaptic LTP, increasing q only, did not yield as reliable synaptic transmission (blue curve in Figure 2c,d) — maximal reliability required presynaptic LTP in addition. This is because, the variance of the first postsynaptic response increases quadratically with the postsynaptic factor q (see Material and methods). Our learning rule compensates for this increase in variance by also increasing the presynaptic factor P, thus making postsynaptic responses reliable and easier to discriminate. The increased discriminability does not only hold for the first response, but generalizes when considering the sum of the first k EPSPs. Furthermore, the benefit of unified STDP remained when we compared the temporal information transmission across a range of presynaptic frequencies (Figure 2 - figure supplement 3) [25, 26].

The change in SNR and variability is consistent with recent sensory perception experiments [27] in which pairing a tone with nucleus basalis stimulation led to an increased mean and a decreased variability of synaptic responses (Figure 2 - figure supplement 2). Mapped to the parameters of the model, both q and P of the potentiated *on* responses increased (see Material and methods). Conversely, *off* responses that were depressed, decreased in P and did not significantly change in q (Figure 2 - figure supplement 2), consistent with the initial modifications that the model predicts (Figure 2c). Therefore, unified pre- and postsynaptically expressed plasticity can account for the improved sensory perception after learning observed experimentally [27]. Furthermore our model suggests that both pre- and postsynaptic components should depend on sensory experience, in agreement with prior findings [28, 29].

Figure 2: Unified pre- and postsynaptic plasticity improves receptive field discriminability. (**a**) Synaptic input rates follow a Gaussian spatial profile (solid grey line). Initially, the presynaptic factor P (top) and the postsynaptic factor q (bottom) are uniformly distributed (dashed lines). After learning, P (top) and q (bottom) both follow the input profile. Dark and light red crosses define examples of *on* and *off* receptive field positions, respectively. (**b**) After learning, the signal-to-noise ratio (SNR) is increased for *on* and decreased for *off* neurons. Postsynaptic plasticity alone leads to a smaller improvement (blue line). (**c**) While *on* neurons obtain higher SNR for postsynaptic-only potentiation (dark blue arrows), unified pre- and postsynaptic potentiation yields considerably better SNR (dark red arrows). *Off* neurons get lower SNR in both scenarios (light blue and light red arrows). Modifications of *in-vivo* synaptic responses to a tone from *on* and *off* receptive field positions (dark and light green arrows, respectively; reanalyzed from [27], see Material and methods) are consistent with unified pre- and postsynaptic expression but not with postsynaptic expression alone. The black square represents starting condition. Arrows represent the plasticity trajectory, where the model trajectories are plotted every 50 ms. (**d**) Only *on* positions with both pre- and postsynaptic plasticity yield near-perfect discrimination (dark red). Shown for comparison, the discrimination before development (black), after development for *off* neurons (light red), and after development for *on* neurons with postsynaptic expression only (blue).

Plasticity should also allow the organism to quickly adapt to changing environments. Expression of layer-5 pyramidal cell STDP is curiously asymmetric: LTP is both pre- and postsynaptic [7], whereas LTD is expressed only presynaptically on the slice experiments timescale [21]. In addition, presynaptic modifications are stronger than postsynaptic LTP (Figure 1d-e). To explore the consequences of this asymmetry, we extended the above network to study development when high rate inputs alternate between two locations. The neuron learned each receptive field by changes in the presynaptic factor P and the postsynaptic factor q (Figure 3a-c). When the stimulus location changed, however, the postsynaptic memory trace decayed only very slowly as a result of homeostatic scaling (Figure 3b). As a result, the neuron could rapidly relearn the previously acquired receptive field by just increasing P , which amounted to a ten-fold decrease in time to learn (Figure 3d,e). Unified pre- and postsynaptically expressed STDP thus allows for learning of new information while retaining hidden traces of prior experience.

Interestingly, spine changes in layer-5 pyramidal cells of visual cortex outlast sensory experience [30], thus providing a structural substrate for the psychological phenomenon known as memory savings [31]. As synaptic structure and synaptic weight are closely correlated [32, 33], the memory savings mediated by structural spine plasticity [30] are reminiscent of those provided by our unified plasticity model.

Here we have focused on neocortical data. Models based on synaptic traces are flexible and can describe both neocortical and hippocampal plasticity data [14, and Appendix 1]. We therefore expect that our modelling framework should also be able to capture plasticity in other brain regions, although with different parameters. For example, there are several key differences in the expression locus and in the speed of pre- and postsynaptic changes in hippocampus [6]. In cerebellum, there is evidence for the opposite asymmetry of expression, with LTP being pre- and postsynaptic, but LTD only postsynaptic [34, 35].

In our work, memory savings are a consequence of the postsynaptic weight decay occurring on a much slower timescale than the presynaptic modifications. This arrangement, however, is not crucial for the predicted rapid relearning. What is necessary is that the synaptic strength is the product of pre- and postsynaptic components ($w = Pq$) and that these components evolve on different timescales. For example, fast postsynaptic changes combined with slow presynaptic changes would allow for the corresponding presynaptic trace of previous experience, which indeed could be the case in the cerebellum [34, 35]. Taken together, these findings suggest that plasticity expression asymmetry is not particular to neocortical layer-5 pyramidal cells, but rather a general functional principle that extends across different brain regions. Interestingly, similar functions can also be performed by neuronal inhibition, to sharpen receptive fields [36], to keep hidden memories in recurrent neural networks [37], and to act as a substrate for memory savings in the cerebellum [38].

Figure 3: Unified pre- and postsynaptic STDP displays rapid relearning of previously experienced stimuli. (**a**) The presynaptic factor P follows the switching between two stimuli (red and blue profiles, arrows indicate switching time-points). (**b**) The postsynaptic factor q, however, is not erased and a trace of previously learned information remains, which decays slowly only due to synaptic homeostasis. The neuron was initially tuned to the red stimulus. The initial learning of the blue stimulus (at 1s) was slow, but much faster the second time (at 101s). (**c**) The neuron's tuning follows the two stimuli, as indicated by the alternating stimulus-specific spiking. Previously experienced stimuli are forgotten by the postsynaptic neuron, but a hidden trace remains. (**d**) Relearning occurs faster than learning. (**e**) Relearning was an order of magnitude faster than initial learning (time to reach 99% performance).

The existence of both pre- and postsynaptic expression of long-term synaptic plasticity has been enigmatic. Although it has been known that changes in release probability play a key role in determining the transmission of information across synapses [39, 40, 18], our theoretical treatment is the first to show that combined pre- and postsynaptic expression of long-term synaptic plasticity provides the brain with reliable sensory detection and the ability to quickly relearn previously experienced stimuli.

Acknowledgments

We thank Gary Bhumbra, Megan Carey, Claudia Clopath, Wulfram Gerstner, Matthias Hennig, Miha Pelko, Jean-Pascal Pfister, Paolo Puggioni, Walter Senn, Lukas Solanka, the Sjï¿œstrï¿œm lab, the Vogels lab and the Center for Neural Circuits and Behaviour for useful discussions. We thank Michelle Giugliano for sharing his code to calculate synaptic information transmission with dynamic synapses.

Material and methods

Short- and Long-term Synaptic Plasticity model

Short-term plasticity model

To model short-term synaptic plasticity, we used the Tsodyks-Markram model with facilitation [22]. This model is defined by the following ODEs

$$\frac{dr(t)}{dt} = \frac{1-r(t)}{D} - p(t)r(t)X(t), \tag{1}$$
$$\frac{dp(t)}{dt} = \frac{P-u(t)}{F} + P[1-p(t)]X(t). \tag{2}$$

The first equation models the vesicle depletion process, where the (normalized) number of vesicles r is decreased with an amount $p(t)r(t)$ after a presynaptic spike from the train $X(t) = \sum_{t_{pre}} \delta(t - t_{pre})$. Between spikes r recovers to 1 with a depression time constant D. The second equation models the dynamics of the presynaptic factor p which increases an amount $P[1-p]$ after every presynaptic spike, decaying back to baseline presynaptic factor P with a facilitation time constant F. By varying the synaptic dynamics parameters D, F and P, one can obtain different synaptic dynamics. We used typical values for pyramidal-onto-pyramidal synapses [41], $D = 200$ms and $F = 50$ms, while P is modified by long-term plasticity as below. The average number of vesicles released per spike is $r(t)p(t)$, which can be interpreted as the presynaptic strength.

Long-term plasticity model

In layer-5 pyramidal to pyramidal cell synapses, timing-dependent long-term depression (LTD) is presynaptically expressed. It is mediated by the coincidence between a postsynaptic signal (endocannabinoid release) and a presynaptic signal (presynaptic NMDA receptor activation) [21, 42, 43, 8]. LTP is driven by postsynaptic coincidence detection of the combined binding of glutamate and postsynaptic depolarization [43, 7, 44], promoting an increase in the number and/or properties of postsynaptic AMPA receptors [45]. However, timing-dependent long-term potentiation (LTP) also has a presynaptic component, mediated by postsynaptic diffusion of nitric oxide (NO) [46, 7, 47, 8].

Our phenomenological triplet model of long-term modification of pre- and postsynaptic components has three synaptic traces, two postsynaptic (y_+ and y_-) and one presynaptic (x_+), which increase upon a post- or presynaptic spike, respectively (see Appendix 1 for a more detailed comparison with the triplet model [14]). The traces are obtained by filtering the spike trains with a first-order low-pass filter. We defined the postsynaptic depression trace

$$\frac{dy_-(t)}{dt} = \frac{-y_-(t)}{\tau_{y_-}} + Y(t), \tag{3}$$

the postsynaptic potentiation trace

$$\frac{dy_+(t)}{dt} = \frac{-y_+(t)}{\tau_{y_+}} + Y(t), \tag{4}$$

and the presynaptic potentiation trace

$$\frac{dx_+(t)}{dt} = \frac{-x_+(t)}{\tau_{x_+}} + X(t). \tag{5}$$

The long-term modification in the weight is achieved by modifying the postsynaptic factor q and the presynaptic factor P. The postsynaptic factor is modified with every postsynaptic spike Y according to

$$\Delta q = c_+ \underbrace{x_+(t)y_-(t-\epsilon)Y(t)}_{\text{Triplet}^{\text{LTP}}_{\text{post}}}, \tag{6}$$

where c_+ is a constant that sets the amount of postsynaptic LTP. The y_- trace is evaluated at $(t-\epsilon)$, so that the value of the respective synaptic trace is readout before being updated. The triplet character of this rule is expressed by the fact that it contains the presynaptic component once, but the postsynaptic activity twice (Y and filtered version y_-). This ensures that LTP only takes place when the postsynaptic spike follows both a presynaptic spike and a preceding postsynaptic spike [14]. As a result, low pairing frequencies do not lead to LTP, as y_- will have decayed, consistent with data [23].

Similarly, the presynaptic factor is modified whenever the presynaptic cell is active according to

$$\Delta P = -d_- \underbrace{y_-(t)y_+(t)X(t)}_{\text{Triplet}^{\text{LTD}}_{\text{pre}}} + d_+ \underbrace{x_+(t-\epsilon)y_+(t)X(t)}_{\text{Triplet}^{\text{LTP}}_{\text{pre}}}. \tag{7}$$

For plasticity in P to occur, the presynaptic spikes X readout the postsynaptic traces (presynaptic coincidence detection), y_-y_+ for presynaptic LTD and x_+y_+ for presynaptic LTP. d_- and d_+ are constants that set the amount of presynaptic LTD and LTP, respectively. While presynaptic LTD has a triplet form, it contains two postsynaptic traces and the raw presynaptic spike train. Therefore it does not vanish at low frequencies. Equivalently, this term could be written as a doublet rule with a double exponential as the presynaptic trace.

The total synaptic strength is a product of both pre- and postsynaptic factors

$$w(t) = qp(t)r(t). \tag{8}$$

For a synapse that has not been stimulated recently this simplifies to $w = Pq$.

Being a probability we hard-bounded $P = [0, 1]$. The postsynaptic factor q had a lower bound of 0, and an upper bound of 2. Alternatively a soft-bounded rule could be used [48]. In the data used to fit the model (see below), postsynaptic homosynaptic LTD was not apparent on the timescale of the experiment. Because it seems unrealistic that the postsynaptic factor q never decreases, slow homeostasic scaling of the postsynaptic factor was included for network simulations [24]. This prevents weakly active synapses from potentiating the postsynaptic factor q. It was modelled as a postsynaptic subtractive normalization, so that the total change in q of synapse i was equal to $\Delta q_i - \alpha \frac{1}{N} \sum_{j=1}^{N} \Delta q_j$ [49]. The only condition on the speed α for it to be consistent with the data, is that it should not lead to noticable homeostasis on the timescale of the experiments. For computational efficiency we used $\alpha = 0.075$, which is still orders of magnitude faster than what has been observed in homeostasis experiements. The exact form of slow normalization ($\alpha \to 0$) does not affect the qualitative behavior of the model. Note that the timescale of the slow normalization determines how long the memory savings effects are present.

To speed up the numerical implementations, we integrated the synaptic traces between the pre- and postsynaptic spikes. In the following equations, we label the presynaptic spikes with k and the postsynaptic ones with l.

$$y_-^{l+1} = y_-^l \exp\left(-\frac{\Delta t_{post}}{\tau_{y_-}}\right) + 1, \tag{9}$$

$$y_+^{l+1} = y_+^l \exp\left(-\frac{\Delta t_{post}}{\tau_{y_+}}\right) + 1, \tag{10}$$

$$x_+^{k+1} = x_+^k \exp\left(-\frac{\Delta t_{pre}}{\tau_{x_+}}\right) + 1. \tag{11}$$

We subsequently integrated the model between pre- and postsynaptic spikes

$$q_{l+1} = q_l + c_+ x_+^k \exp\left(-\frac{\Delta t_{post-pre}}{\tau_{x_+}}\right) y_-^l \exp\left(-\frac{\Delta t_{post}}{\tau_{y_-}}\right), \tag{12}$$

$$P_{k+1} = P_k - d_- y_-^l \exp\left(-\frac{\Delta t_{pre-post}}{\tau_{y_-}}\right) y_+^l \exp\left(-\frac{\Delta t_{pre-post}}{\tau_{y_+}}\right), \tag{13}$$

$$+ d_+ y_+^l \exp\left(-\frac{\Delta t_{pre-post}}{\tau_{y_+}}\right) x_+^k \exp\left(-\frac{\Delta t_{pre}}{\tau_{x_+}}\right), \tag{14}$$

where $\Delta t_{post-pre}$ is the time between the current postsynaptic spike and the last presynaptic spike, Δt_{post} is the time between the current postsynaptic (presynaptic) spike and the last one, and similarly for $\Delta t_{pre-post}$ and Δ_{pre}. Finally, we also integrated the STP equations (Eqs. 1 and 2) between presynaptic spikes k and $k+1$, a time Δt_{pre} apart, yielding

$$r_{k+1} = 1 - [1 - r_k(1 - u_k)] \exp\left(-\frac{\Delta t_{\text{pre}}}{D}\right), \tag{15}$$

$$p_{k+1} = P + p_k [1 - P] \exp\left(-\frac{\Delta t_{\text{pre}}}{F}\right), \tag{16}$$

with initial conditions $r_0 = 1$ and $p_0 = P$.

Model fitting to *in-vitro* plasticity data

We fitted the free parameters of the long-term plasticity model $\boldsymbol{\theta} = \{d_-, \tau_{y_-}, d_+, \tau_{y_+}, c_+, \tau_{x_+}\}$ to the frequency- and timing-dependent slice STDP data of layer-5 pyramidal cells [23]. Parameters are shown in Table 1. Rather than fitting to changes in the weight w, we fitted directly to modifications in P and q (see Eqs. 21 and 22 for our estimators of P and q). This was done by minimizing the mean squared error between the data and the experiments for both P and q (as shown in Figure 1)

$$\boldsymbol{\theta} = \text{argmin}_{\boldsymbol{\theta}} \frac{1}{N} \sum_j^N \left[\left(\frac{P_{\text{model}}^{\text{after}}}{P_{\text{model}}^{\text{before}}} - \frac{P_{\text{data}}^{\text{after}}}{P_{\text{data}}^{\text{before}}} \right)^2 + \left(\frac{q_{\text{model}}^{\text{after}}}{q_{\text{model}}^{\text{before}}} - \frac{q_{\text{data}}^{\text{after}}}{q_{\text{data}}^{\text{before}}} \right)^2 \right], \tag{17}$$

where N denotes the number of protocols fitted, 10 in total (5 different pairing frequencies with -10 ms or $+10$ ms relative timing, see below). For induction protocols at high frequencies ($>$10 Hz), pre- and postsynaptic spike trains consisted of five spikes that were paired 15 times at 0.1 Hz. Low-frequency pairings (0.1 Hz) were done with a single pre- and postsynaptic spike (as in [23]). Before plasticity induction, P and q were set to 0.5 and 1, respectively. For the interaction of STP and STDP simulations (Figure 1f, g), we used a standard passive neuron model with a membrane time constant of 25ms.

Parameter	d_-	τ_{y_-} (ms)	d_+	τ_{y_+} (ms)	c_+	τ_{x_+} (ms)
Young rat visual cortex	0.1771	32.7	0.1548	230.2	0.0618	66.6

Table 1: Unified pre- and postsynaptic STDP model parameters. The model was fitted to data from young rat visual cortex [23].

Without further fitting this model also captured pharmacological blockade of the plasticity traces. In the model, we simulated the experimental effects of pharmacological blockade by setting the relevant parameter or variable to 0. Specifically, we simulated the effects of blocking two different retrograde messenger systems shown to be involved in STDP in layer-5 pyramidal cell pairs, endocannabinoid signaling [21] and nitric oxide signaling [7]. To reproduce pharmacological blockade experiments, we used high-frequency pairing (50 Hz) with +10 ms delay, which is comparable with our frequency-dependent results and approximates the long depolarizing currents used in [7]. Blocking endocannabinoid receptors prevents presynaptic LTD [21]. By setting $d_- = 0$ presynaptic LTD was disabled. This reveals presynaptic LTP and enhances short-term depression (Figure 1 - figure supplement 3), consistent with experimental evidence [7], as the drugs used are likely to block presynaptic endocannabinoid receptors. In contrast, blocking nitric oxide decreases LTP but does not affect short-term synaptic dynamics [7] (Figure 1 - figure supplement 3a). We simulated this by setting $y_+ = 0$, so that both presynaptic components were absent.

Stochastic synaptic responses and *in-vitro* P and q estimation

The release of neurotransmitter was assumed to follow a standard binomial model [50]

$$P_{\mathrm{syn}}(X = k) = \binom{N}{k} P^k (1-P)^{N-k}, \tag{18}$$

which defines the probability of having k successful events (neurotransmitter release) given N trials (release sites) with equal probability P.

The mean synaptic response is scaled by a postsynaptic factor q, which can be related to the quantal amplitude so that

$$\mu_{\mathrm{syn}} = PqN, \tag{19}$$

and the variance is

$$\sigma^2_{\text{syn}} = q^2 NP(1-P). \tag{20}$$

Following the binomial release model (Eq. 18), μ_{syn} (Eq. 19) and σ^2_{syn} (Eq. 20),

$$P = \frac{\mu_{\text{syn}}}{Nq}, \tag{21}$$

and

$$q = \frac{\sigma^2_{\text{syn}}}{\mu_{\text{syn}}} + \frac{\mu_{\text{syn}}}{N}. \tag{22}$$

The number of release sites N is believed to change only after a few hours [51, 52]. As the slice synaptic plasticity experiments analysed here lasted only up to 1.5 hours [23] and we were interested in the relative changes we assumed constant $N = 5.5$ in our analysis below, as estimated in [53] using data from the same connection type we used to fit our model. Eqs. 21 and 22 were used to estimate P and q from *in-vitro* plasticity data (see above), respectively (dataset deposited at Dryad data repository with DOI doi:10.5061/dryad.p286g [54]). Note that because the data had to be reanalized in full there are minor differences in the mean weights previously published [23].

We verified our P and q extraction method by analysing short-term plasticity experiments with pharmacological manipulation of presynaptic release or of postsynaptic gain [Fig S1a, 21], and experiments with pharmacological blockade of pre- or postsynaptic long-term plasticity [Figure S1b, 7] (Figure 1 - figure supplement 2a,b). In addition, long-term changes in P but not in q were inversely correlated with changes in paired-pulse ratio, as expected (Figure 1 - figure supplement 2c,d). Taken together, these results lend experimental support to our binomial-distribution-based approach for extracting P and q to tune changes in the pre- and postsynaptic modifications of our unified STDP model (Figure 1d,e).

Analysis of *in-vivo* data

We extracted the effective P and q from the *in-vivo* data obtained by [27]. Again using a binomial model, we obtained estimators for their variability measure given by $v = q(1-P)$ and the mean by $\mu = PqN$. To ease comparison with our simulations we set the initial P to the same initial condition used in our simulations $P = 0.5$ [41]. We then obtained the initial $N = \frac{|\mu|}{qP}$ and the initial $q = \frac{q}{(1-P)}$. For the after pairing data we allowed both pre- and postsynaptic factors P and q to change, while N was fixed to the values extracted before pairing [51]. The estimations after learning were obtained as $q = q + \frac{|\mu|}{N}$ and $P = \frac{|\mu|}{Nq}$. We used these estimators to extract q and P from measurements for both the depression experienced for the unpaired (best before pairing) receptive field position and the potentiated paired position [27]. After pairing, the effective q of the potentiated ('on') response increased from $q^{\text{on}}_{\text{before}} = 23.3\text{pA}$ to $q^{\text{on}}_{\text{after}} = 27.1\text{pA}$ (+16.3%), while P increased from $P^{\text{on}}_{\text{before}} = 0.5$ to $P^{\text{on}}_{\text{after}} = 0.73$ (+46%). Responses that were depressed ('off'), typically the original best frequency, yielded no statistically significant change in $q^{\text{off}}_{\text{before}}$, while $P^{\text{off}}_{\text{before}} = 0.5$ and $P^{\text{off}}_{\text{after}} = 0.40$ (-20%) (Figs. 2, 2 - figure supplement 1 and 2 - figure supplement 2). To ease comparison with the postsynaptic factor in the simulations we scaled the experimentally obtained q such that before plasticity it was 1. We compared models where we allowed both P and q to change or only one of them, the lower variability estimation error was the one where both factors change (2 - figure supplement 2e). The estimation error was calculated as $\frac{1}{N}\sum_i^N (v^i_{\text{real}} - v^i_{estimated})^2$, where N is the number of data points.

Synaptic signal detection

We calculated the Signal-to-Noise Ratio (SNR) of a synaptic response defined here by a random variable s, amidst additive background noise defined by the random variable n as follows

$$\text{SNR}_{syn} = 2\frac{(\langle s\rangle - \langle n\rangle)^2}{\sigma_s^2 + \sigma_n^2} \tag{23}$$

It is assumed that $n \sim \mathcal{N}(0, \sigma_n^2)$ and we also used the Gaussian approximation to the binomial release model specified above, $s \sim \mathcal{N}(PqN, q^2NP(1-P) + \sigma_n^2)$, from which follows the SNR of the first postsynaptic response

$$\text{SNR}_{syn} = 2\frac{(PqN)^2}{q^2NP(1-P) + 2\sigma_n^2} \tag{24}$$

In Figure 2, we used $\sigma_n^2 = 0.5$. Variance of the k-th postsynaptic response is given by $\sigma^2_{\text{syn}^\text{k}} = q^2Nr_kp_k(1 - r_kp_k)$ (Figure 2 - figure supplement 3a). The SNR of the k-th postsynaptic response is

$$\text{SNR}^k_{syn} = 2\frac{(r_kp_kqN)^2}{q^2Nr_kp_k(1-r_kp_k) + 2\sigma_n^2} \tag{25}$$

where p_k and r_k are given by Eqs. 16 and 15, respectively. The SNR of the sum of the first K responses, evoked at a given presynaptic firing rate ρ therefor equals

$$\mathrm{SNR}^{\rho}_{syn} = 2\frac{\left(\sum_{k=0}^{K-1} r_k p_k q N\right)^2}{\sum_{k=0}^{K-1} q^2 N r_k p_k(1-r_k p_k) + 2\sum_{k=0}^{K-1}\sigma_n^2} \tag{26}$$

After unified STDP the first response has a higher release probability but the second one a much lower probability due to synaptic depression. Combined with the background noise, the SNR can drop when the second or further responses are included. However, the SNR of the summed response will always be larger than when only post-synaptic modifications are made (see Figure 2 - figure supplement 3b). This holds for any frequency, Figure 2 - figure supplement 3c and carries over to an information theoretic analysis of the response, Figure 2 - figure supplement 3d.

Next, we used ROC analysis to compute the *false alarm* and *detection* probability of the first postsynaptic response

$$p_{\text{false alarm}} = \int_T^{+\infty} P_n(r)dr = \frac{1}{2}\,\mathrm{erfc}\left(\frac{T}{\sqrt{2\sigma_n^2}}\right) \tag{27}$$

$$p_{\text{detection}} = \int_T^{+\infty} P_s(r)dr = \frac{1}{2}\,\mathrm{erfc}\left(\frac{T - PqN}{\sqrt{2q^2NP(1-P)+\sigma_n^2}}\right) \tag{28}$$

where T is the discrimination threshold, and erfc is the complementary error function defined as $\mathrm{erfc}(x) = \frac{2}{\sqrt{\pi}}\int_x^{\infty} e^{-t^2}dt$. To assess the overall discriminability, we used $p_{\text{discrimination}}$, which is the area under the ROC curve (AUC). The AUC was computed by integrating over the ROC curve using the trapezoid method (see Figure 2d). Given that N is a simple constant we set it to 1, unless otherwise stated (see data inference above).

Receptive field development

For the receptive field development simulations, we used a feedforward network with 100 presynaptic neurons j with Poisson statistics and a single integrate-and-fire postsynaptic neuron. The postsynaptic neuron was modelled as an adaptive exponential integrate-and-fire neuron model [55]. Model parameters were as reported in [55] and synapses were modelled as input currents. The firing rate of the presynaptic Poisson neurons was modelled using a Gaussian profile, defined as

$$\rho(j;p,\sigma) = \rho_{\min} + (\rho_{\max} - \rho_{\min})\mathrm{e}^{\frac{-(j-p)^2}{2\sigma^2}} \tag{29}$$

where ρ is the rate in the Poisson neuron model j, p the input position for which the rate is maximal, and $\sigma = 5$ Hz the distribution spread. ρ_{max} and ρ_{min} are the maximum and minimum rates, and were set to $\rho_{\rm max} = 50$ Hz and $\rho_{\rm min} = 3$ Hz. We scaled d_-, d_+ and c_+ by a factor 0.15 to yield a smoother receptive field development. q was bounded between 0 pA and 200 pA, so that the synaptic input is appropriately scaled for the neuron model used. The network was simulated for 100s to achieve convergence. For the memory savings experiment, we interleaved two receptive field positions. Results for receptive development and memory savings were averaged over 10 runs. The response of the postsynaptic neuron (Figure 3c) was assessed by presenting each stimulus alone with long-term synaptic plasticity inactive. Receptive field simulations were implemented in simulator Brian 2.0 [56]. Code for running and plotting the savings experiment is available online [1].

Statistical comparison

Results are reported as mean ± SEM. Statistical comparisons were made with Student's t test for equal means, if data was normally distributed as assessed using Kolmogorov-Smirnov test, Mann-Whitney U non-parametric test was used otherwise. For multiple comparisons we applied ANOVA or Kruskal-Wallis test for normally or non-normally distributed data, respectively. For correlation analysis the Spearman's coefficient was used together with one-tailed Student's t test. Significance levels are $*p < 0.05$, $**p < 0.01$, and $***p < 0.001$.

[1] https://senselab.med.yale.edu/ModelDB/ShowModel.cshtml?model=XXX

Supplemental Figures

Figure 1 - figure supplement 1: The unified pre- and postsynaptic STDP model (blue solid line) captured the characteristic temporal asymmetry of experimental STDP (black squares represent data from [23]). Relative timing was defined as $\Delta t = t_{\text{post}}^{\text{spike}} - t_{\text{pre}}^{\text{spike}}$. Pairing frequency was 0.1 Hz (left), 20 Hz (middle) and 50 Hz (right).

Figure 1 - figure supplement 2: Extraction of P and q from synaptic plasticity data from slice paired recordings using pharmacology and high frequency pairing (based on a long-step current injection plasticity protocol). (**a**) The AMPA/kianate antagonist CNQX decreased q ($p < 0.01$), but not P ($p = 0.32$; red symbols), while low bath calcium decreased P ($p < 0.01$), but not q ($p = 0.48$; blue symbols). Control experiments did not yield changes in either component: P ($p = 0.15$) and q ($p = 0.1$; black symbols) (data reanalyzed from [21]). (**b**) Extraction of P and q after LTP induction and blockade of plasticity traces with nitric oxide (NO) and endocannabinoids (eCB). LTP induction (control; black symbols) yielded an increase in both P ($p < 0.001$) and q ($p < 0.001$). eCB blockade increased the presynaptic factor P ($p < 0.01$), but did not change q ($p = 0.1$; blue symbols), while LTP induction under NO blockade increased q ($p < 0.001$), but did not change P ($p = 0.27$; red symbols) (data reanalyzed from [7]). (**c**,**d**) Changes in presynaptic factor P (**c**), but not postsynaptic factor q (**d**) correlated with changes in paired-pulse ratio. Dashed line represents a linear regression on the individual data points (open circles). Data shown was normalized to baseline (before plasticity induction). Open symbols represent individual experiments, while solid symbols in (a) and (b) represent averages. Error bars represent SEM.

Figure 1 - figure supplement 3: Model is consistent with modifications of synaptic dynamics after pharmacological blockade of plasticity traces. (**a**) After LTP induction under nitric oxide (NO) blockade (top), no changes in synaptic dynamics were observed when blocking NO retrograde signalling, in keeping with the model results (bottom). (**b**) Strong depression is revealed after endocannabinoids (eCB) blockade (top), similar to the model (bottom). Data was reproduced from [7]. Data shown was normalized to the maximum amplitude before and after plasticity induction to highlight changes in the synaptic dynamics.

Appendix 1

Title: Comparison between unified pre- and postsynaptic STDP model, and triplet STDP model [14]

Legend: In this appendix we compare and discuss the similarities and differences between our model and the triplet STDP model [14].

Figure 2 - figure supplement 1: Long-term pre- and postsynaptic plasticity reduces response variability of receptive fields. (**a**) After receptive field development synaptic variance dropped for both *on* and *off* neurons. (**b**) Synaptic variance as a function of P and q (grey colour map). Black square represents initial condition. As in (a), after development *on* and *off* neurons yielded low synaptic variance (dark and light red arrows, respectively). *In-vivo* plasticity results measuring synaptic responses from *on* and *off* receptive fields are in agreement with modelling predictions (data from [27] – green arrows). For comparison, the results for a learning rule where only the postsynaptic factor is modified for *on* and *off* neurons (dark and light blue arrows, respectively). (**c**) Probability of discrimination (area under the curve in Figure 2d) for different background noise levels. Solid black line represents the initial condition. Black dashed line represents a random classifier, while grey dashed line represents the background noise level used in Figure 2.

Figure 2 - figure supplement 2: Extraction of effective P and q from *in-vivo* receptive field plasticity experiments (data reanalyzed from [27]). (**a**) Modification of variability and mean as reported in [27] after stimulation of nucleus basalis. Data is shown for both unpaired (referred to as *off* the receptive field) frequencies (mean: blue filled circles, single experiments: light blue circles) and paired (referred to as *on* the receptive field) frequencies (mean: red filled circles, single experiments: light red circles) receptive fields. (**b**) Modification in P and q for *on* and *off* positions, obtained using a standard binomial release model on the synaptic responses recorded by [27] (see Material and methods). (**c**) After receptive field plasticity q did not change in *off* positions ($p = 1$), but was upregulated in *on* ($p < 0.05$) positions. (**d**) P was also downregulated and upregulated for *off* ($p < 0.05$) and *on* ($p < 0.001$) positions, respectively, after receptive field plasticity. (**e**) An estimator where both P and q change yielded the lowest variability estimation error, compared to estimators where P or q were fixed.

Figure 2 - figure supplement 3: Long-term pre- and postsynaptic plasticity improves signal-to-noise ratio (SNR) and information transmission in dynamic synapses. (**a**) Model with both pre- and postsynaptic plasticity reduces synaptic transmission variability with dynamic synapses (top, red line), while postsynaptic plasticity alone increases variability (bottom, blue line). Black line represents initial condition as in Figs. 2c. Shaded area represents the variance of the postsynaptic response. (**b**) The SNR of the sum of multiple pulses is improved across in the unified model (red line), compared to postsynaptic plasticity alone (red line; see Material and methods). The presynaptic firing rate is 30 Hz in (a) and (b). (**c**) In analogy with the SNR of the first response (Figs. 2c), the SNR of the sum of the first 15 responses across different presynaptic frequencies is better for the unified model compared to postsynaptic plasticity alone. (**d**) Synaptic information transmission [25, 26] for the unified model across different presynaptic frequencies is better than with postsynaptic plasticity alone.

References

[1] Pawlak, V., Greenberg, D. S., Sprekeler, H., Gerstner, W. & Kerr, J. N. Changing the responses of cortical neurons from sub- to suprathreshold using single spikes in vivo. *eLife* **2** (2013).

[2] Nabavi, S. *et al.* Engineering a memory with LTD and LTP. *Nature* (2014).

[3] MacDougall, M. J. & Fine, A. The expression of long-term potentiation: reconciling the preists and the postivists. *Philosophical Transactions of the Royal Society B: Biological Sciences* **369**, 20130135–20130135 (2013).

[4] Padamsey, Z. & Emptage, N. Two sides to long-term potentiation: a view towards reconciliation. *Philosophical Transactions of the Royal Society B: Biological Sciences* **369**, 20130154 (2014).

[5] Zakharenko, S., Zablow, L. & Siegelbaum, S. Visualization of changes in presynaptic function during long-term synaptic plasticity. *Nature Neuroscience* **4**, 711–717 (2001).

[6] Bayazitov, I. T., Richardson, R. J., Fricke, R. G. & Zakharenko, S. S. Slow presynaptic and fast postsynaptic components of compound long-term potentiation. *The Journal of neuroscience : the official journal of the Society for Neuroscience* **27**, 11510–11521 (2007).

[7] Sjöström, P. J., Turrigiano, G. G. & Nelson, S. Multiple forms of long-term plasticity at unitary neocortical layer 5 synapses. *Neuropharmacology* **52**, 176–184 (2007).

[8] Yang, Y. & Calakos, N. Presynaptic long-term plasticity. *Frontiers in Synaptic Neuroscience* **5** (2013).

[9] Loebel, A., Le Bé, J.-V., Richardson, M. J. E., Markram, H. & Herz, A. V. M. Matched pre- and post-synaptic changes underlie synaptic plasticity over long time scales. *The Journal of neuroscience : the official journal of the Society for Neuroscience* **33**, 6257–6266 (2013).

[10] Gerstner, W., Kempter, R., van Hemmen, J. & Wagner, H. A neuronal learning rule for sub-millisecond temporal coding. *Nature* **383**, 76–78 (1996).

[11] Song, S., Miller, K. & Abbott, L. F. Competitive Hebbian learning through spike-timing-dependent synaptic plasticity. *Nature Neuroscience* (2000).

[12] Senn, W., Markram, H. & Tsodyks, M. An algorithm for modifying neurotransmitter release probability based on pre-and postsynaptic spike timing. *Neural Computation* **13**, 35–67 (2001).

[13] Seung, H. S. Learning in Spiking Neural Networks by Reinforcement of Stochastic Synaptic Transmission. *Neuron* **40**, 1063–1073 (2003).

[14] Pfister, J.-P. & Gerstner, W. Triplets of spikes in a model of spike timing-dependent plasticity. *Journal of Neuroscience* **26**, 9673–9682 (2006).

[15] Froemke, R. C., Tsay, I. A., Raad, M., Long, J. D. & Dan, Y. Contribution of individual spikes in burst-induced long-term synaptic modification. *Journal of Neurophysiology* **95**, 1620–1629 (2006).

[16] Leibold, C. & Bendels, M. H. K. Learning to discriminate through long-term changes of dynamical synaptic transmission. *Neural Computation* **21**, 3408–3428 (2009).

[17] Clopath, C., Büsing, L., Vasilaki, E. & Gerstner, W. Connectivity reflects coding: a model of voltage-based STDP with homeostasis. *Nature Neuroscience* **13**, 344–352 (2010).

[18] Carvalho, T. P. & Buonomano, D. V. A novel learning rule for long-term plasticity of short-term synaptic plasticity enhances temporal processing. *Frontiers in integrative neuroscience* **5**, 20 (2011).

[19] Graupner, M. & Brunel, N. Calcium-based plasticity model explains sensitivity of synaptic changes to spike pattern, rate, and dendritic location. *Proceedings of the National Academy of Sciences* **109**, 3991–3996 (2012).

[20] Albers, C., Schmiedt, J. T. & Pawelzik, K. R. Theta-specific susceptibility in a model of adaptive synaptic plasticity. *Frontiers in Computational Neuroscience* **7** (2013).

[21] Sjöström, P. J., Turrigiano, G. G. & Nelson, S. B. Neocortical LTD via coincident activation of presynaptic NMDA and cannabinoid receptors. *Neuron* **39**, 641–654 (2003).

[22] Markram, H., Wang, Y. & Tsodyks, M. Differential signaling via the same axon of neocortical pyramidal neurons. *Proc. Natl. Acad. Sci. USA* **95**, 5323–5328 (1998).

[23] Sjöström, P. J., Turrigiano, G. G. & Nelson, S. B. Rate, Timing, and Cooperativity Jointly Determine Cortical Synaptic Plasticity. *Neuron* **32**, 1149–1164 (2001).

[24] Turrigiano, G. G., Leslie, K. R., Desai, N. S., Rutherford, L. C. & Nelson, S. B. Activity-dependent scaling of quantal amplitude in neocortical neurons. *Nature* **391**, 892–896 (1998).

[25] Fuhrmann, G., Segev, I., Markram, H. & Tsodyks, M. Coding of temporal information by activity-dependent synapses. *Journal of Neurophysiology* **87**, 140–148 (2002).

[26] Testa-Silva, G. *et al.* High bandwidth synaptic communication and frequency tracking in human neocortex. *PLoS Biology* **12**, e1002007 (2014).

[27] Froemke, R. C. *et al.* Long-term modification of cortical synapses improves sensory perception. *Nature Neuroscience* **16**, 79–88 (2013).

[28] Finnerty, G. T., Roberts, L. S. & Connors, B. W. Sensory experience modifies the short-term dynamics of neocortical synapses. *Nature* **400**, 367–371 (1999).

[29] Cheetham, C. E. J., Barnes, S. J., Albieri, G., Knott, G. W. & Finnerty, G. T. Pansynaptic enlargement at adult cortical connections strengthened by experience. *Cerebral cortex (New York, N.Y. : 1991)* **24**, 521–531 (2014).

[30] Hofer, S., Mrsic-Flogel, T., Bonhoeffer, T. & Hübener, M. Experience leaves a lasting structural trace in cortical circuits. *Nature* **457**, 313–317 (2008).

[31] Ebbinghaus, H. Memory: A contribution to experimental psychology. *Teachers College, Columbia University* (1913).

[32] Matsuzaki, M. *et al.* Dendritic spine geometry is critical for AMPA receptor expression in hippocampal CA1 pyramidal neurons. *Nature Neuroscience* **4**, 1086–1092 (2001).

[33] Holtmaat, A. & Svoboda, K. Experience-dependent structural synaptic plasticity in the mammalian brain. *Nature Reviews Neuroscience* **10**, 647–658 (2009).

[34] Wang, Y. T. & Linden, D. J. Expression of cerebellar long-term depression requires postsynaptic clathrin-mediated endocytosis. *Neuron* **25**, 635–647 (2000).

[35] Lev-Ram, V., Mehta, S. B., Kleinfeld, D. & Tsien, R. Y. Reversing cerebellar long-term depression. *Proc. Natl. Acad. Sci. USA* **100**, 15989–15993 (2003).

[36] Wilson, N. R., Runyan, C. A., Wang, F. L. & Sur, M. Division and subtraction by distinct cortical inhibitory networks in vivo. *Nature* – (2012).

[37] Vogels, T. P., Sprekeler, H., Zenke, F., Clopath, C. & Gerstner, W. Inhibitory Plasticity Balances Excitation and Inhibition in Sensory Pathways and Memory Networks. *Science* **334**, 1569–1573 (2011).

[38] Medina, J. F., Garcia, K. S. & Mauk, M. D. A mechanism for savings in the cerebellum. *The Journal of neuroscience : the official journal of the Society for Neuroscience* **21**, 4081–4089 (2001).

[39] Otmakhov, N., Shirke, A. M. & Malinow, R. Measuring the impact of probabilistic transmission on neuronal output. *Neuron* **10**, 1101–1111 (1993).

[40] Stevens, C. F. & Wang, Y. Changes in reliability of synaptic function as a mechanism for plasticity. *Nature* **371**, 704–707 (1994).

[41] Costa, R. P., Sjostrom, P. J. & van Rossum, M. C. W. Probabilistic inference of short-term synaptic plasticity in neocortical microcircuits. *Frontiers in Computational Neuroscience* **7**, 75 (2013).

[42] Sjöström, P. J., Turrigiano, G. G. & Nelson, S. B. Endocannabinoid-dependent neocortical layer-5 LTD in the absence of postsynaptic spiking. *Journal of Neurophysiology* **92**, 3338–3343 (2004).

[43] Bender, V. A. & Feldman, D. Two Coincidence Detectors for Spike Timing-Dependent Plasticity in Somatosensory Cortex. *The Journal of neuroscience : the official journal of the Society for Neuroscience* **26**, 4166–4177 (2006).

[44] Shouval, H. Z., S-HWang, S. & MWittenberg, G. Spike timing dependent plasticity: a consequence of more fundamental learning rules. *Frontiers in Computational Neuroscience* 1–13 (2010).

[45] Malinow, R. & Malenka, R. C. AMPA receptor trafficking and synaptic plasticity. *Annual Review of Neuroscience* **25**, 103–126 (2002).

[46] Hardingham, N. & Fox, K. The role of nitric oxide and GluR1 in presynaptic and postsynaptic components of neocortical potentiation. *The Journal of neuroscience : the official journal of the Society for Neuroscience* **26**, 7395 (2006).

[47] Hardingham, N., Dachtler, J. & Fox, K. The role of nitric oxide in pre-synaptic plasticity and homeostasis. *Frontiers in Cellular Neuroscience* **7** (2013).

[48] van Rossum, M. C. W., Shippi, M. & Barrett, A. B. Soft-bound synaptic plasticity increases storage capacity. *PLOS Computational Biology* **8**, e1002836 (2012).

[49] Miller, K. D. & MacKay, D. J. The role of constraints in Hebbian learning. *Neural Computation* **6**, 100–126 (1994).

[50] Del Castillo, J. & Katz, B. Quantal components of the end-plate potential. *The Journal of physiology* **124**, 560–573 (1954).

[51] Bolshakov, V. Y., Golan, H., Kandel, E. R. & Siegelbaum, S. A. Recruitment of New Sites of Synaptic Transmission During the cAMP-Dependent Late Phase of LTP at CA3–CA1 Synapses in the Hippocampus. *Neuron* **19**, 635–651 (1997).

[52] Saez, I. & Friedlander, M. J. Plasticity between Neuronal Pairs in Layer 4 of Visual Cortex Varies with Synapse State. *The Journal of neuroscience : the official journal of the Society for Neuroscience* **29**, 15286–15298 (2009).

[53] Markram, H., Lübke, J., Frotscher, M., Roth, A. & Sakmann, B. Physiology and anatomy of synaptic connections between thick tufted pyramidal neurones in the developing rat neocortex. *The Journal of physiology* **500 (Pt 2)**, 409–440 (1997).

[54] Costa, R., Froemke, R., Sjöström, P. & van Rossum, M. Data from: Unified pre- and postsynaptic long-term plasticity enables reliable and flexible learning (2015).

[55] Brette, R. & Gerstner, W. Adaptive exponential integrate-and-fire model as an effective description of neuronal activity. *Journal of Neurophysiology* **94**, 3637 (2005).

[56] Goodman, D. & Brette, R. Brian: a simulator for spiking neural networks in python. *Frontiers in neuroinformatics* **2**, 5 (2008).

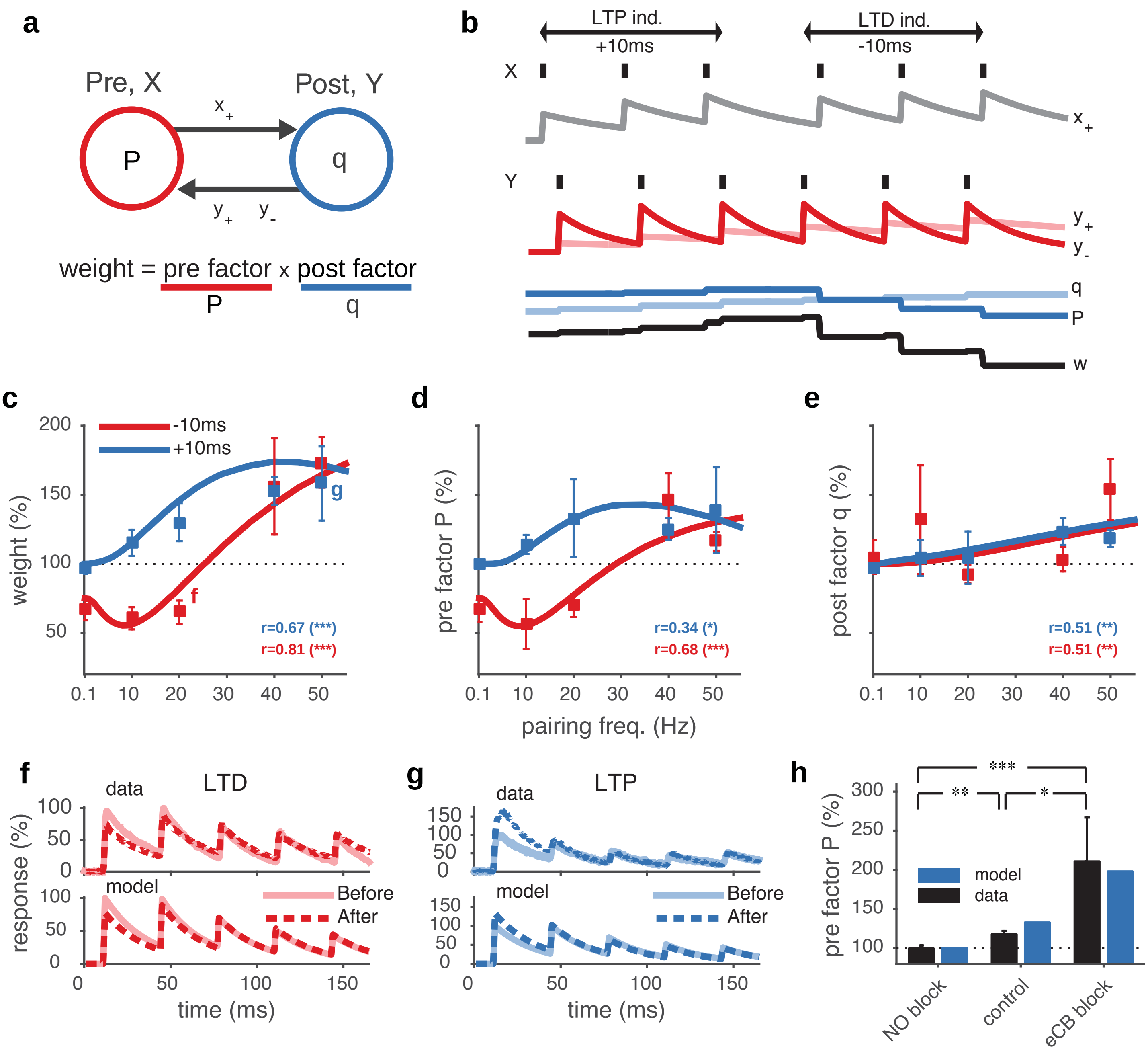

a
Pre, X
Post, Y
P
q
x+
y+ y-
weight = pre factor x post factor
P
q
b
LTP ind.
+10ms
LTD ind.
-10ms
X
Y
x+
y+
y-
q
P
w
c
-10ms
+10ms
weight (%)
r=0.67 (***)
r=0.81 (***)
d
pre factor P (%)
r=0.34 (*)
r=0.68 (***)
e
post factor q (%)
r=0.51 (**)
r=0.51 (**)
pairing freq. (Hz)
f
data
LTD
model
Before
After
response (%)
time (ms)
g
data
LTP
model
Before
After
time (ms)
h
pre factor P (%)
model
data
NO block
control
eCB block

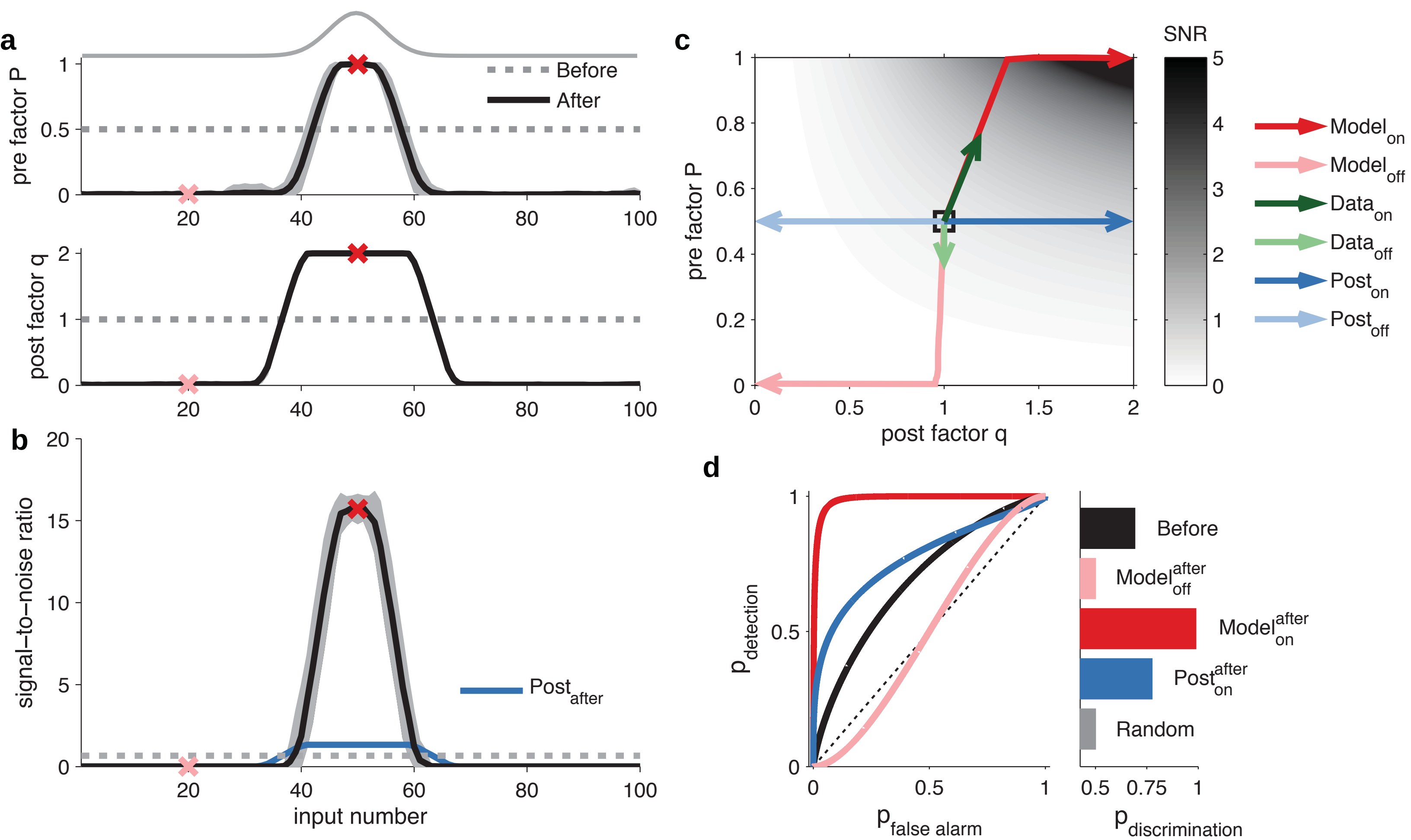
a
b
c
d
pre factor P
post factor q
signal-to-noise ratio
input number
Before
After
Post$_{after}$
SNR
post factor q
pre factor P
Model$_{on}$
Model$_{off}$
Data$_{on}$
Data$_{off}$
Post$_{on}$
Post$_{off}$
$p_{detection}$
$p_{false\ alarm}$
Before
Model$^{after}_{off}$
Model$^{after}_{on}$
Post$^{after}_{on}$
Random
$p_{discrimination}$

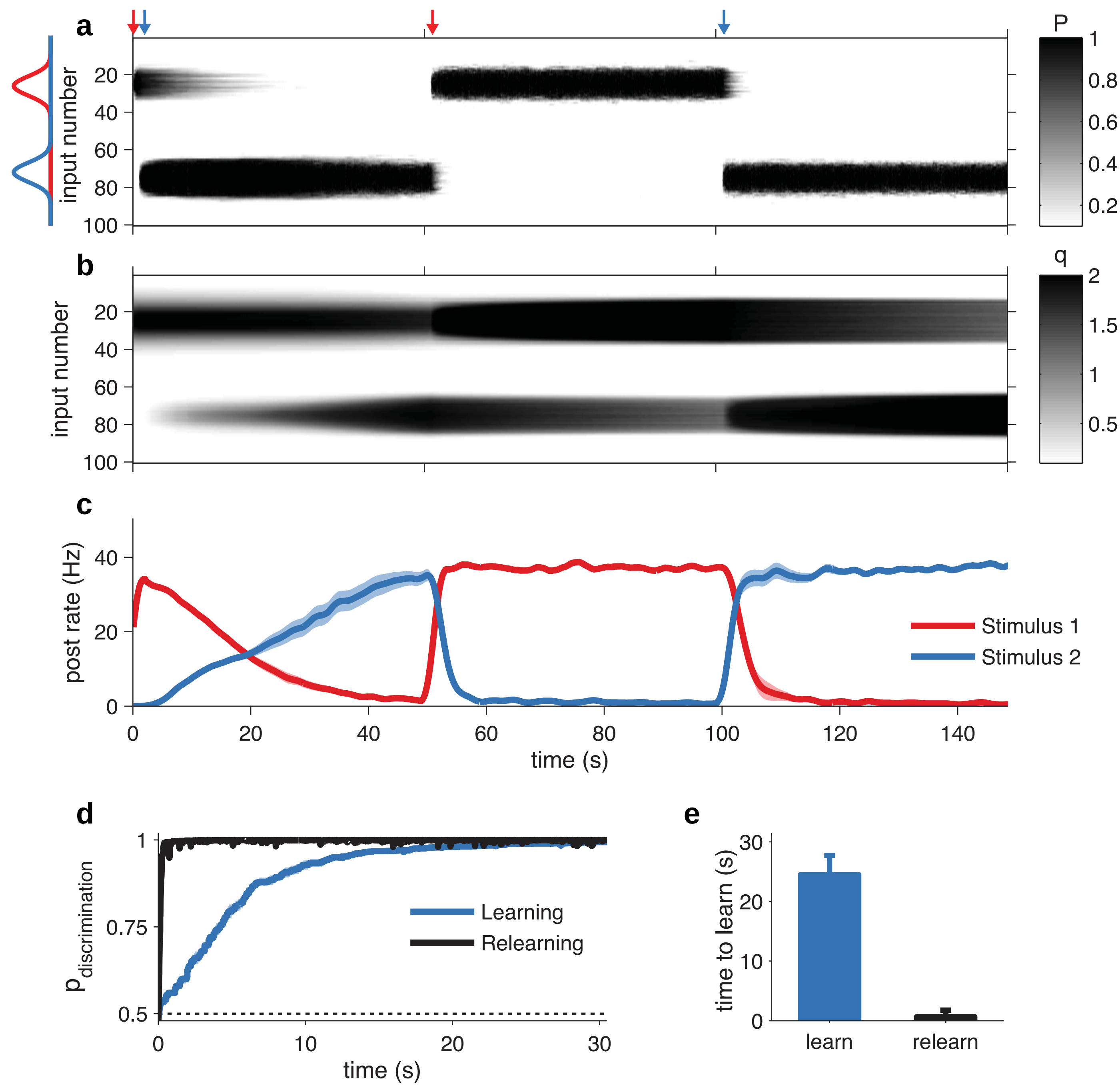
a
b
c
d
e
P
q
input number
post rate (Hz)
time (s)
Stimulus 1
Stimulus 2
$p_{discrimination}$
Learning
Relearning
time to learn (s)
learn
relearn